Obrabotka metallov (tekhnologiya, oborudovanie, instrumenty) = Metal Working and Material Science. 2025 vol. 27 no. 4 pp. 272–286
ISSN: 1994-6309 (print) / 2541-819X (online)
DOI: 10.17212/1994-6309-2025-27.4-272-286

NSTU NETI

Obrabotka metallov - Metal Working and Material Science

Journal homepage: http://journals.nstu.ru/obrabotka_metallov

Effect of Zr, Sc, and Hf additions on the microstructure formation of cast ALTEK alloys

Alina Levagina [1, a, *], ***Evgenii Aryshenskii*** [1, b], ***Sergey Konovalov*** [1, c], ***Dmitry Rasposienko*** [2, d]

[1] Siberian State Industrial University, 42 Kirova str., Novokuznetsk, 654007, Russian Federation
[2] M.N. Miheev Institute of Metal Physics of Ural Branch of Russian Academy of Sciences, 18 S. Kovalevskoy st., Yekaterinburg, 620990, Russian Federation

[a] https://orcid.org/0000-0002-7270-6008, levagina_aa@sibsiu.ru; [b] https://orcid.org/0000-0003-3875-7749, arishenskiy_ev@sibsiu.ru;
[c] https://orcid.org/0000-0003-4809-8660, konovalov@sibsiu.ru; [d] https://orcid.org/0000-0002-7670-9054, dmitrijrasp@gmail.com

ARTICLE INFO

Article history:
Received: 14 August 2025
Revised: 16 September 2025
Accepted: 25 October 2025
Available online: 15 December 2025

Keywords:
Aluminum alloys
ALTEK
Al-Cu-Mn-Mg
Structure modification
Grain structure
Cast microstructure
X-ray diffraction analysis
Scanning electron microscopy

Funding
The study was funded by the Russian Science Foundation grant No. 24-19-00064, https://rscf.ru/project/ 24-19-00064/.

ABSTRACT

Introduction. Aluminum alloys of the *Al-Cu-Mn* system, alloyed with 23% copper and 1–2% manganese (*ALTEK*), are distinguished by heat resistance and high mechanical properties due to the formation of nano-dispersed particles of the $Al_{20}Cu_2Mn_3$ phase. When exposed to high temperatures (up to 400°C), the particles block the processes of polygonization and recovery, hindering the movement of grain boundaries. A promising direction for improving these alloys is the modification of the cast structure with transition metals (*TMs*). An insufficient content of *TMs* does not provide a modifying effect, while an excessive amount leads to a reduction in strength due to the formation of a large number of coarse intermetallic particles. **The subject** of this work a *ALTEK* alloys alloyed with *Mg*, *Zr*, *Sc*, and *Hf*. **The purpose** of the work is to determine the optimal concentrations of scandium, hafnium, and zirconium required for effective modification of the cast structure of *ALTEK* alloys during complex alloying. The effect of complex additions of transition metals (*Zr*, *Sc*, *Hf*) on the formation of the cast structure of *Base0.15Zr0.05Sc0.05Hf*, *Base0.1Zr0.14Sc0.16Hf*, *Base0.1Zr0.2Sc0.16Hf, and Base0.1Zr0.25Sc0.16Hf* alloys is investigated in comparison to the base alloy. **The research methods** were optical and scanning electron microscopy, and X-ray diffraction analysis. **Results and discussion.** Modification of the grain structure in alloys with a scandium content of less than 0.20% is not observed, and the average grain structure size is 350 μm. The addition of scandium in the amount of 0.20% and 0.25% leads to a decrease in the average grain diameter to 41.8 μm and 29.7 μm, respectively. Scanning electron microscopy showed that particles of the Al_6Mn and Al_2CuMg phases are present in all the alloys studied. Particles of the $Al_3(Sc,Hf,Zr)$ phase are found in the *Base0.1Zr0.2Sc0.16Hf* and *Base0.1Zr0.25Sc0.16Hf* compositions. X-ray diffraction analysis revealed the $Al_{20}Cu_2Mn_3$ phase and small amounts of Al_6Mn and Al_2CuMg in the base alloy and in the *Base0.1Zr0.25Sc0.16Hf* alloy. The structural modification is explained by the precipitation of primary $Al_3(Sc, Zr, Hf)$ particles. **Application of the results.** The obtained results are promising for the development of new materials for the manufacture of aerospace products. **Conclusions.** The addition of 0.20–0.25% scandium with a zirconium content of 0.1% and hafnium of 0.16% is the most effective.

For citation: Levagina A.A., Aryshenskii E.V., Konovalov S.V., Rasposienko D.Yu. Effect of Zr, Sc, and Hf additions on the microstructure formation of cast ALTEK alloys. *Obrabotka metallov (tekhnologiya, oborudovanie, instrumenty) = Metal Working and Material Science*, 2025, vol. 27, no. 4, pp. 272–286. DOI: 10.17212/1994-6309-2025-27.4-272-286. (In Russian).

Introduction

The combination of low density and high corrosion resistance makes aluminum a high-demand material. Its alloys, modified with alloying elements and thermomechanical treatment, provide excellent mechanical and performance characteristics, making them indispensable in the aerospace, automotive, and power generation industries [1, 2].

ALTEK alloys of the *Al-Cu-Mn* system, which possess above-average thermal stability, are of particular scientific and practical interest. Such alloys are characterized by a low copper content (1–3 %) compared

*** Corresponding author**
Levagina Alina A., junior researcher
Siberian State Industrial University,
42 Kirova str.,
654007, Novokuznetsk, Russian Federation
Tel.: +7 900 321-55-05, **e-mail:** levagina_aa@sibsiu.ru

to industrial alloys, and the manganese content varies within the 1–2 % range. A two-phase structure, consisting of an aluminum solid solution and a thermally stable $Al_{20}Cu_2Mn_3$ phase, is formed in these alloys [3–5]. Nanosized $Al_{20}Cu_2Mn_3$ particles effectively suppress recrystallization and recovery processes at temperatures up to 400 °C during prolonged exposure (at least 3 hours) [6–8]. One method for improving the structural and functional properties of *ALTEK* alloys is to modify their as-cast microstructure.

Fine-grained structures exhibit enhanced plasticity and strength and are less prone to low-temperature brittleness. In contrast, coarse-grained structures degrade the performance and service properties of rolled sheets due to non-uniform deformation and increase the rejection rate [9]. Fine-grain structure formation is facilitated by high cooling rates, physical effects (e.g., ultrasound), the introduction of modifying additives, and thermomechanical treatment parameters. However, crystallization at high cooling rates and the application of physical effects are not always feasible in production. Therefore, the use of modifying agents is the most practical method for grain refinement during casting [10].

Transition metals (*TMs*) are the most commonly used modifying agents [11–17]. Scandium (*Sc*), as the most effective modifying agent, forms primary Al_3Sc particles that act as crystallization nuclei. However, the high cost of *Sc* necessitates alternative solutions. It has been experimentally established that the combined addition of *Zr* and *Hf* allows for a reduction in *Sc* content while enhancing the modifying effect [11]. The aspect of combined *Zr*, *Sc*, and *Hf* addition has been insufficiently studied for *ALTEK* system alloys. Existing studies have addressed the effects of *Zr* [6, 18] and *Zr* and *Sc* (with *Cr* addition) [7]; however, the effect of *Hf* addition has not been investigated.

Studies [6, 19, 20] mention the effect of zirconium addition on the properties of *ALTEK* alloys. Typically, zirconium content varies within the 0.22–0.59 *Zr* range (compositions: *1.97% Cu-1.92% Mn-0.22% Zr; 1.48% Cu-1.53% Mn-0.41% Zr; 1.11% Cu-0.95% Mn-0.59% Zr* [6, 19]; *1.6% Cu-1.37% Mn-0.5% Zr* [18]). However, unlike the base compositions, zirconium had a negligible effect on the as-cast structure in the above alloys, as it was fully dissolved in the aluminum solid solution in the as-cast state. Study [21] examined an alloy with *Sc* addition (*1.74% Cu-1.57% Mn-0.25% Zr-0.1% 1Sc*). This alloy exhibits an as-cast structure similar to that of ternary *Al-Cu-Mn* alloys. Al_7Cr particles were identified in [7] for an *Al-Cu-Mn-(Sc, Cr)* alloy (*1.6% Cu–1.8% Mn–0.4% Zr–0.15% Cr*). The grain structure consists of two zones: columnar and equiaxed crystals, which may also be associated with crystallization in a small-diameter (40 mm) graphite mold. It should be noted that in all the studied compositions, the selection of rare earth metals was aimed at preventing the formation of primary intermetallic compounds; therefore, the TMs did not significantly affect the as-cast structure. Primary Al_3Sc- and Al_3Zr-type intermetallic compounds, in turn, have a dual function: on one hand, they act as modifying agents, refining the grain structure and thereby improving strength properties according to the *Hall-Petch* relationship [22]; on the other hand, such intermetallic compounds act as stress concentrators, often leading to a reduction in plasticity in the alloys containing them. For this reason, in practical applications, efforts are made to select transition element concentrations that, on one hand, ensure as-cast structure refinement and, on the other hand, do not cause the formation of large amounts of primary intermetallic compounds. However, such studies have not been conducted for *ALTEK* alloys.

Thus, ***the objective of this study*** is to determine the optimal *Sc*, *Hf*, and *Zr* concentrations required for effective as-cast structure modification during complex alloying of *ALTEK* alloys. The following ***tasks*** will be addressed to achieve this objective:

1. Comparative analysis of grain structures.

2. Identification of intermetallic compounds formed in the studied *ALTEK* alloys using scanning electron microscopy and X-ray diffraction analysis.

Methods

It is known that for effective grain structure modification of aluminum alloys, the combined amount of *Sc* and *Zr* should not exceed 0.11–0.15 % [16], and *Hf* addition is effective if its maximum content is 0.2 % [11]. These guidelines were observed to select the transition metal contents.

The phase composition was analyzed using computational methods with the *Thermo-Calc* software and the *TTAL5* database. The alloy phase composition was simulated at temperatures of 200 and 400 °C.

Casting

Five alloys with the chemical compositions listed in Table 1 were cast in a steel chill mold to investigate the effect of the *TM* complex.

Table 1

Chemical composition of model alloys

No.	Content, %					
	Cu	*Mn*	*Mg*	*Zr*	*Sc*	*Hf*
1	2	2	1.5	–	–	–
2	2	2	1.5	0.15	0.05	0.05
3	2	2	1.5	0.1	0.14	0.16
4	2	2	1.5	0.1	0.20	0.16
5	2	2	1.5	0.1	0.25	0.16

The following designations were introduced for convenience:

- ***Base*** – base alloy ***2% Cu-2% Mn-1.5% Mg***
- ***Base0.15Zr0.05Sc0.05Hf***
- **Base0.1Zr0.14Sc0.16Hf**
- ***Base0.1Zr0.2Sc0.16Hf***
- ***Base0.1Zr0.25Sc0.16Hf***

The numbers preceding the chemical symbols indicate their concentration in weight percent (wt.%).

The ingots were produced by melting in an induction furnace and casting into a steel chill mold. The melting procedure was performed as described in a previous study [14]. The following materials were used as charge: *A85* grade aluminum, *Mg90* magnesium, *M1* copper, *Al-Sc2, Al-Zr5, Al-Hf2* master alloys, and *Mn90Al10* alloying pellets.

The chemical composition of the produced alloys was determined according to [15]. The sampling for analysis was performed at 730 °C.

Microstructure examination

Optical microscopy was used to assess the efficiency of the selected ratio and concentration of the modifying agents. The microstructure was examined on a smooth, cleaned surface. For metallographic preparation, the samples were mounted in epoxy resin, and the surfaces were ground using a *Forcipol 2* dual-disk grinder/polisher with abrasive papers of varying grit sizes (*P400*, *P600*, *P800*, *P1000*, *P1500*, and *P2000*). Final polishing was achieved using a felt cloth and *Goya* paste. The grain structure was revealed by etching in a 15% *NaOH* solution and subsequently treated with a special reagent for visualization. The reagent composition was as follows: 400 ml hydrochloric acid, 220 ml nitric acid, 50 g copper filings, and 300 ml water. For each sample, two images were captured at magnifications of ×50 and ×200 (or lower, if necessary). The average grain size was measured using the linear intercept method according to *GOST 21073.2*. Microstructure images were obtained using an *OLYMPUS GX-51* optical microscope.

For the examination of Al_6Mn, Al_2CuMg, and $Al_3(Sc,Zr,Hf)$ particles, the sample surfaces were prepared by grinding and polishing after mounting in epoxy resin. The samples were then removed from the resin for further examination using a scanning electron microscope. The particles were examined using a *KYKY EM6900* scanning electron microscope, with 10 images captured per sample. For particle identification, *EDS* analysis data were compared with published data [9, 17, 24–27].

X-ray diffraction analysis

X-ray diffraction analysis was performed using a *BRUKER D8 ADVANCE* diffractometer with *CuKα* radiation (λ = 0.15418 nm) over a 2θ angular range of 20° to 60°, with an exposure time of 10 seconds per point. The data were processed using *DIFFRAC.EVA 4.0* and *DIFFRAC.TOPAS 5.0* software [23].

The phase composition of the samples was determined via X-ray phase analysis. Interplanar distances, calculated from the diffraction peak positions, were compared with the *PDF-2/1202* database.

Transmission electron microscopy (TEM)

The ***Base0.1Zr0.2Sc0.16Hf*** alloy was used for $Al_{20}Cu_2Mn_3$ phase identification via *TEM*. The samples were prepared by mechanical thinning followed by electrolytic thinning. 3 mm diameter disks were punched using an *Ultratonic Disk Cutter*. Electropolishing was performed in an *A2* electrolyte using a *Struers Tenupol* unit. A *PIPS II* ion polishing system was used to remove carbon contamination. Grain structure and phase analyses were performed using standard techniques, including bright-field (*BF*) and dark-field (*DF*) imaging and electron microdiffraction. Phases were identified by correlating their interplanar distances with reference data from the *JCPDS-ICDD* database, followed by chemical analysis. The interplanar distances were calculated based on additional reflections in the electron diffraction patterns.

Results and Discussion

Based on optical microscopy data (Fig. 1), the alloy without *TM* additions exhibits a dendritic grain structure with a grain size of approximately 350 μm. No significant grain refinement was observed in the ***Base0.15Zr0.05Sc0.05Hf*** alloy with a low TM content. The average grain diameter was 239 μm. An initial modifying effect was observed in the ***Base0.1Zr0.14Sc0.16Hf*** alloy, where individual fine grains (up to 35 μm in diameter) appeared against a predominantly coarse-grained as-cast structure, reducing the average grain size to 118 μm.

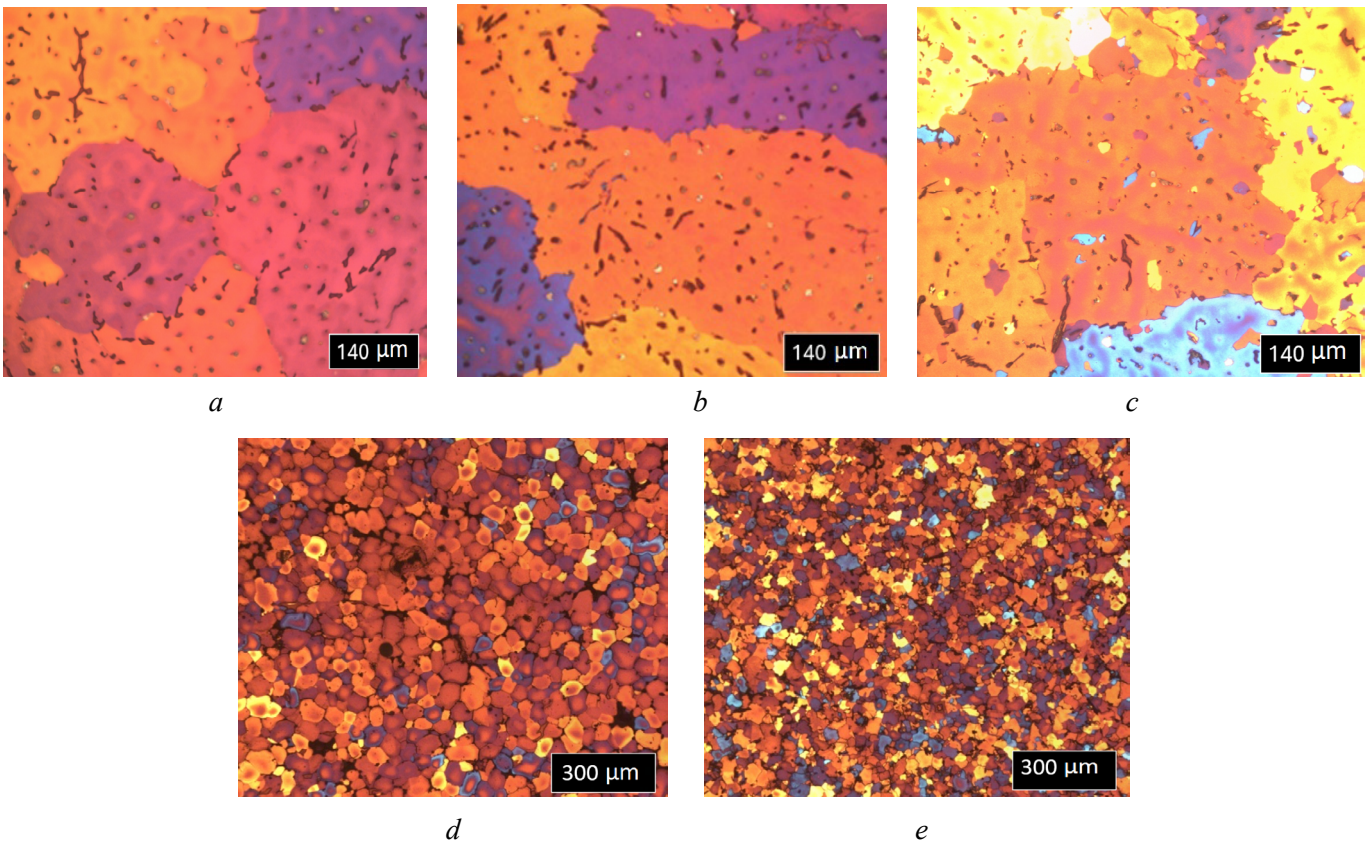

a *b* *c*

d *e*

Fig. 1. Microstructure of *Al-Cu-Mn-Mg* (*Zr*, *Sc*, *Hf*) alloys:

Base (*a*), *Base0.15Zr0.05Sc0.05Hf* (*b*), *Base0.1Zr0.14Sc0.16Hf* (*c*), *Base0.1Zr0.2Sc0.16Hf* (*d*), *Base0.1Zr0.25Sc0.16Hf* (*e*)

Qualitative changes in the microstructure occurred in the ***Base0.1Zr0.2Sc0.16Hf*** and ***Base0.1Zr0.25Sc0.16Hf*** alloys, where effective grain refinement and the formation of an equiaxed grain structure were achieved, likely due to the precipitation of primary *Al₃(Zr,Sc,Hf)* particles. An increase in scandium content from 0.14 to 0.25 % led to a gradual reduction in grain size from 41.8 μm (0.2% *Sc* alloy) to 29.7 μm (0.25% *Sc* alloy).

According to scanning electron microscopy (*SEM*) data, the *Al₆Mn* phase was present in all studied alloys (Figs. 2 and 3). A typical *EDS* spectrum from such an inclusion is shown in Fig. 3, *a*. However, the inclusions exhibited significantly different sizes: their length in the base alloy does not exceed 15 μm (Fig. 2, *a*), while the largest inclusions, with lengths exceeding 45 μm, were identified in the ***Base0.15Zr0.05Sc0.05Hf*** alloy (Fig. 2, *b*). Inclusion sizes in the ***Base0.1Zr0.14Sc0.16Hf*** (Fig. 2, *c*) and ***Base0.1Zr0.25Sc0.16Hf*** (Fig. 2, *f*) alloys are comparable and do not exceed 20–25 μm. Individual large particles up to 40 μm in length were detected in the ***Base0.1Zr0.2Sc0.16Hf*** alloy (Fig. 2, *d*). The presence of the *Al₆Mn* phase in the ***Base*** and ***Base0.1Zr0.2Sc0.16Hf*** alloys was also confirmed by X-ray diffraction analysis (Figs. 4, 5).

All alloys contained *Al₂CuMg* inclusions, with a typical *EDS* spectrum shown in Fig. 3, *b*. Particularly large inclusions, up to 45–60 μm in length, were found in the ***Base0.15Zr0.05Sc0.05Hf*** (Fig. 2, *b*) and ***Base0.1Zr0.2Sc0.16Hf*** (Fig. 2, *e*) alloys. In the ***Base0.1Zr0.25Sc0.16Hf*** alloy, these phase inclusions were smaller, up to 20 μm (Fig. 2, *f*, *g*). In the ***Base*** (Fig. 2, *a*) and ***Base0.1Zr0.2Sc0.16Hf*** (Fig. 2, *e*) alloys, the

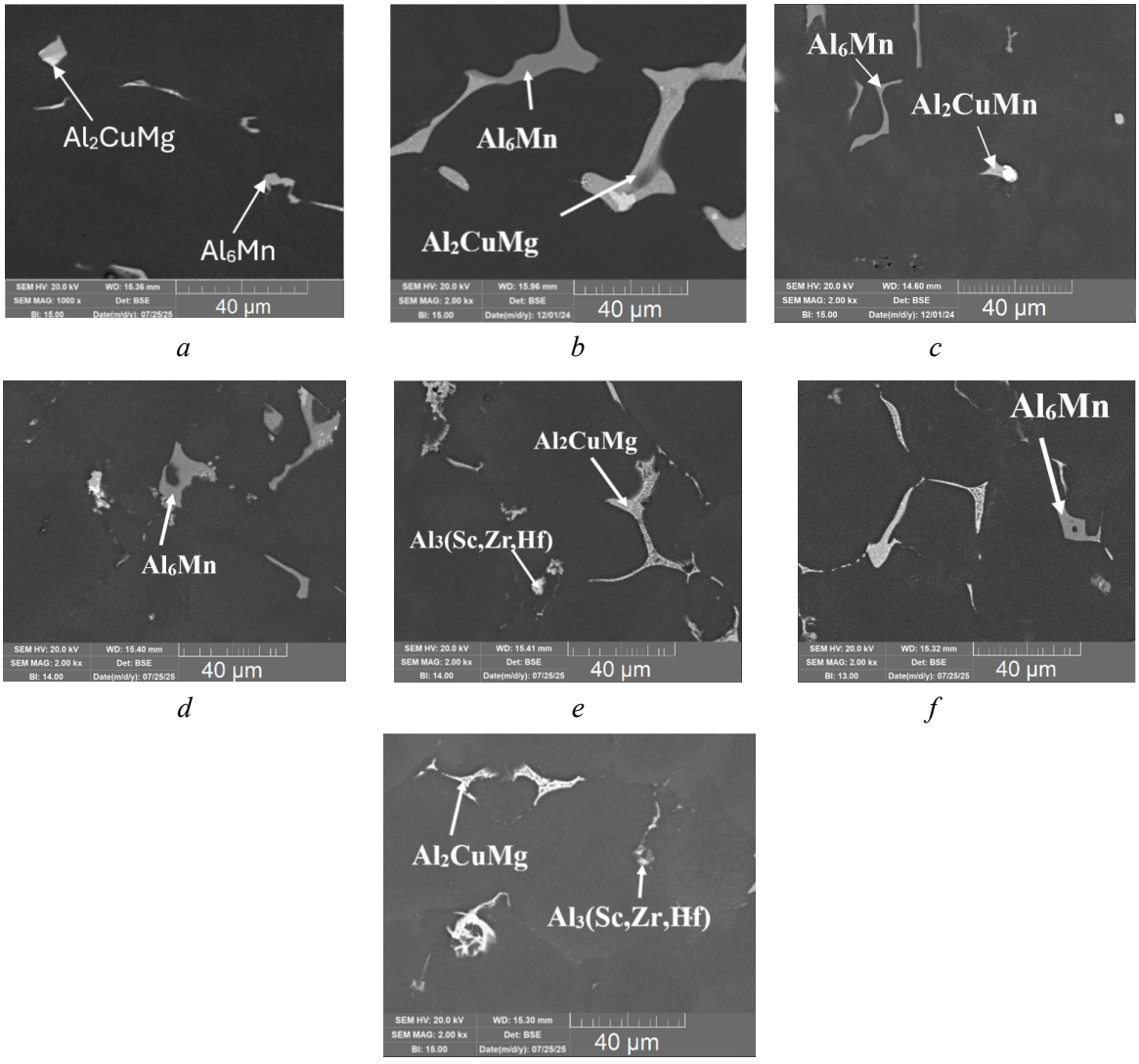

Fig. 2. Microstructure of alloys (*SEM* data):

Base (*a*); *Base0.15Zr0.05Sc0.05Hf* (*b*); *Base0.1Zr0.14Sc0.16Hf* (*c*); *Base0.1Zr0.2Sc0.16Hf* (*d*, *e*); *Base0.1Zr0.25Sc0.16Hf* (*f*, *g*)

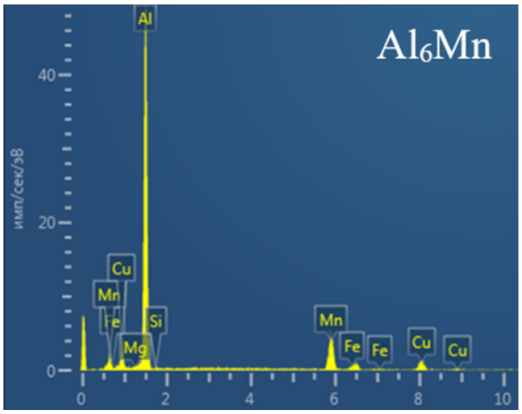

Элемент	Атом. %
Al	78,53
Mn	13,67
Cu	6,39
Si	0,42
Fe	0,88
Mg	0,11

a

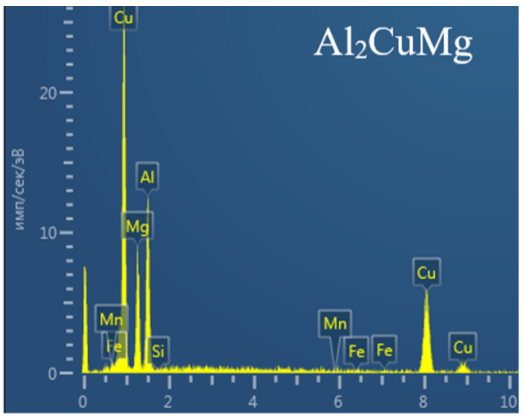

Элемент	Атом. %
Al	37,31
Cu	32,60
Mg	29,36
Si	0,28
Mn	0,23
Fe	0,21

b

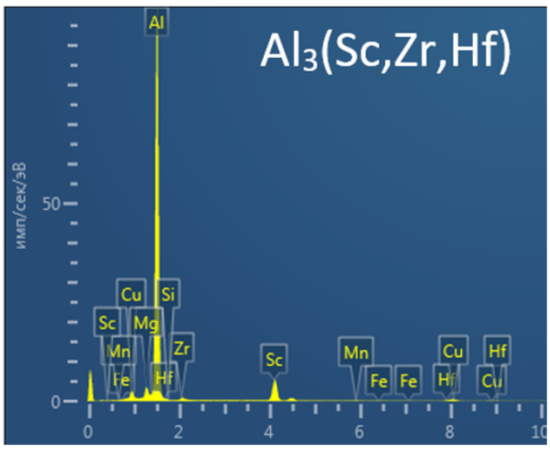

Элемент	Атом. %
Al	86,10
Sc	7,96
Mg	2,44
Cu	1,79
Zr	0,91
Hf	0,38
Si	0,29

c

Fig. 3. Spectrograms of particles in alloys (*EDS* analysis):
Al_6Mn (*a*), *Al_2CuMg* (*b*), *$Al_3(Sc, Zr, Hf)$* (*c*)

inclusion size did not exceed 5–10 μm. The presence of these phases was confirmed by *XRD* analysis of the studied alloys (Figs. 4, 5).

Primary intermetallic compounds *$Al_3(Sc,Zr,Hf)$*, with a near-equiaxed shape and diameters up to 4 μm (Fig. 2, *e*, *g*), were observed in alloys containing 0.2–0.25% *Sc*. A typical *EDS* spectrum from such an inclusion is presented in Fig. 3, *c*. It can be assumed that grain structure refinement is initiated precisely by these primary particles.

According to *XRD* results (Figs. 4, 5), the (*Al*) matrix and *$Al_{20}Cu_2Mn_3$* phase are predominant in the ***Base*** and ***Base0.1Zr0.2Sc0.16Hf*** alloys. Minor amounts of the *Al_2CuMg* and *Al_6Mn* phases were also detected.

The results of phase composition modeling are presented in Fig. 6 and Table 2.

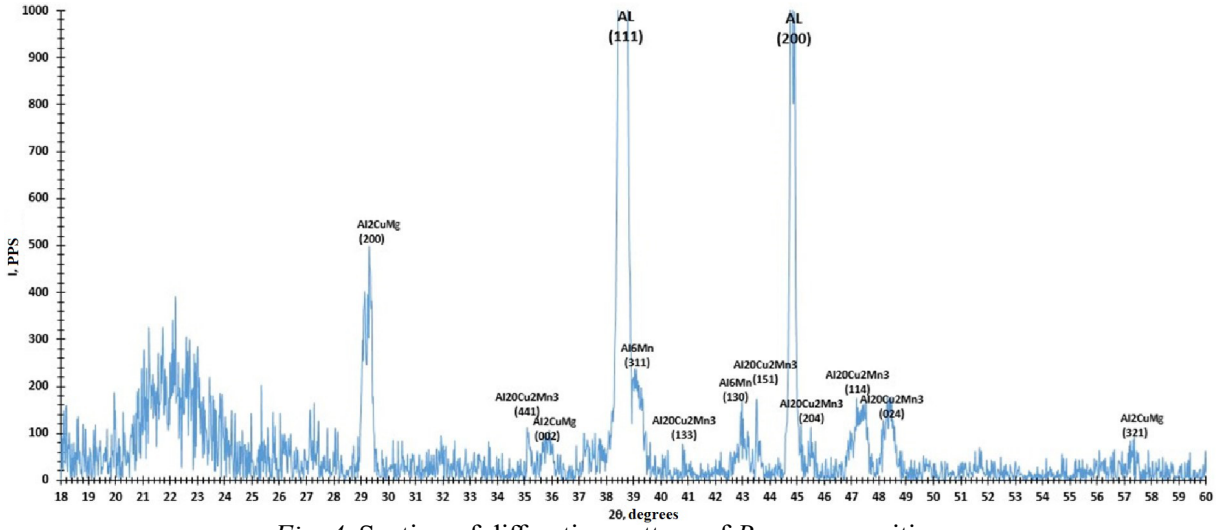

Fig. 4. Section of diffraction pattern of *Base* composition

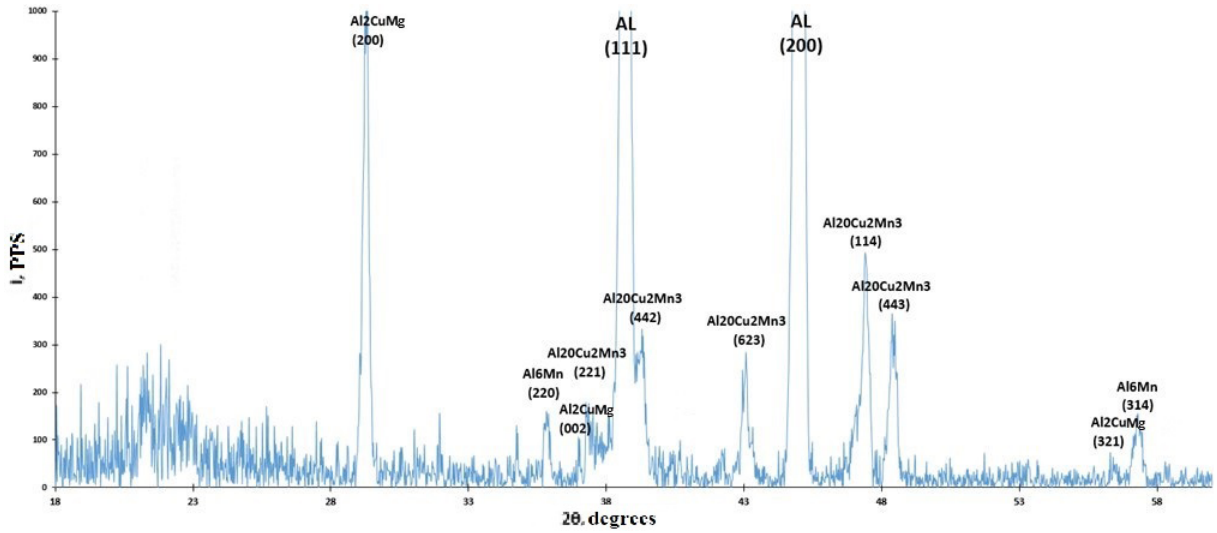

Fig. 5. Section of diffraction pattern of composition *Base0.1Zr0.2Sc0.16Hf*

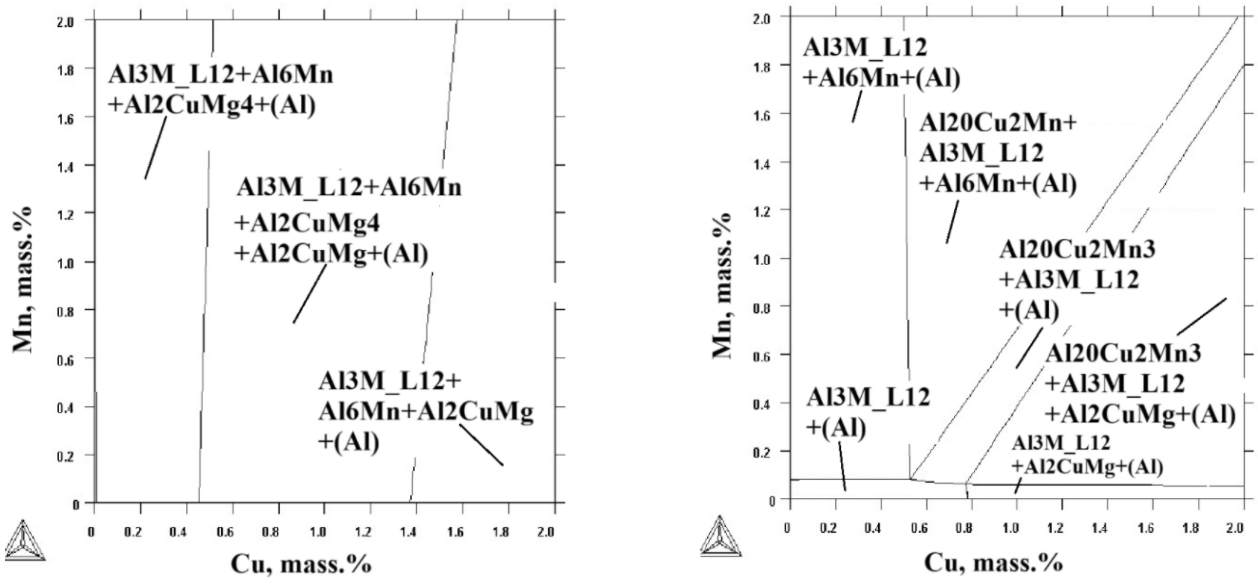

a *b*

Fig. 6. Isothermal sections of the *Base0.1Zr0.14Sc0.16Hf alloy*:
at 200°C (*a*), at 400°C (*b*)

Table 2

Chemical composition of the alloys (*Thermo-Calc*)

No	Chemical composition	Phase composition		
		at 20°C	at 200°C	at 400°C
1	*2% Cu-2% Mn*	$Al_{20}Cu_2Mn_3$+Al_2Cu+(Al)	$Al_{20}Cu_2Mn_3$+ Al_2Cu+(Al)	$Al_{20}Cu_2Mn_3$+(Al)
2	*Base*	$Al_{20}Cu_2Mn_3$+Al_6Mn + + Al_2CuMg+(Al)	$Al_{20}Cu_2Mn_3$+Al_6Mn+ + Al_2CuMg+ (Al)	$Al_{20}Cu_2Mn_3$+(Al)
3	*Base0.15Zr0.05Sc0.05Hf*	$Al_{20}Cu_2Mn_3$+Al_6Mn + + Al_2CuMg $Al_3M\_L1_2$+(Al)	$Al_{20}Cu_2Mn_3$+Al_2CuMg + +Al_6Mn+$Al_3M\_L1_2$+ (Al)	$Al_{20}Cu_2Mn_3$+ + $Al_3M\_L1_2$ +(Al)
4	*Base0.1Zr0.14Sc0.16Hf*	$Al_{20}Cu_2Mn_3$+Al_6Mn+ + Al_2CuMg +$Al_3M\_L1_2$+ (Al)	$Al_{20}Cu_2Mn_3$+Al_2CuMg+ + Al_6Mn+ $Al_3M\_L1_2$+(Al)	$Al_{20}Cu_2Mn_3$+ + $Al_3M\_L1_2$ +(Al)

Modeling demonstrated that ingots of the base alloy have a phase composition consisting of an aluminum solid solution (*Al*), as well as $Al_{20}Cu_2Mn_3$, Al_2CuMg, and Al_6Mn phases. Ingots produced from alloys with *TM* additions (***Base0.15Zr0.05Sc0.05Hf***, ***Base0.1Zr0.14Sc0.16Hf***) contained the Al_3M_L12 phase (where *M* = *Sc*, *Zr*, *Hf*). Thus, the addition of *Mg* to the *2% Cu–2% Mn* alloy leads to the formation of Al_2CuMg and Al_6Mn phases, while the addition of transition metals (*TM*) leads to the formation of a phase with an $L1_2$ (Al_3M_L12) crystal lattice.

Table 3 lists the particles identified in the model alloys and the methods used for their identification. The letter '***M***' indicates that the phase presence was verified by modeling using the *Thermo-Calc* software.

The addition of Mg reduced the grain size. This effect is related to the ability of *Mg* to reduce the interfacial tension in the liquid phase, thereby contributing to an increase in the density of crystallization

Table 3

Particles in the model alloys and methods of their identification

Alloys	Identified particles	Methods
Base	Al_6Mn Al_2CuMg $Al_{20}Cu_2Mn_3$	*SEM,* X-ray diffraction analysis, *M* *SEM,* X- ray diffraction analysis, *M* X-ray diffraction analysis, *M*
Base0.15Zr0.05Sc0.05Hf	Al_6Mn Al_2CuMg $Al_{20}Cu_2Mn_3$	SEM, M
Base0.1Zr0.14Sc0.16Hf	Al_6Mn Al_2CuMg $Al_{20}Cu_2Mn_3$	SEM
Base0.1Zr0.2Sc0.16Hf	Al_6Mn Al_2CuMg $Al_{20}Cu_2Mn_3$ $Al_3(Sc,Zr,Hf)$	*SEM*
Base0.1Zr0.25Sc0.16Hf	Al_6Mn Al_2CuMg $Al_{20}Cu_2Mn_3$ $Al_3(Sc,Zr,Hf)$	*SEM,* X-ray diffraction analysis*, M* *SEM, M* *X-ray* diffraction analysis*, M* *SEM, M*

nuclei. Consequently, the average grain size decreased from 3 mm (in *2% Cu–2% Mn*) to 350 μm (in *2% Cu–2% Mn–1.5% Mg*), confirming the influence of Mg on the crystallization process.

As noted above, a small *TM* addition (***Base0.15Zr0.05Sc0.05Hf***) has an insignificant effect on grain morphology, and the average grain diameter decreases only to 239 μm, while the grains retain an irregular, elongated shape. The ***Base0.1Zr0.14Sc0.16Hf*** composition was characterized by a preserved dendritic structure with an average grain diameter of 118 μm. A transition to a modified, refined structure occurs in alloys with *Sc* contents of 0.20–0.25%, with average grain sizes of 41.8 and 29.7 μm, respectively.

The addition of magnesium in this study led to the formation of Al_2CuMg and Al_6Mn inclusions (e.g., in the ***Base0.15Zr0.05Sc0.05Hf*** composition): magnesium, dissolved in the solid solution, displaces manganese, facilitating the formation of Al_6Mn particles. $Al_{20}Cu_2Mn_3$ phase particles were not detected by *SEM*, likely due to their small size. *TEM* analysis was employed for their identification in the ***Base0.1Zr0.2Sc0.16Hf*** alloy (Fig. 7). The identified particles had an elongated, axis-symmetric shape and a length of approximately 200 nm.

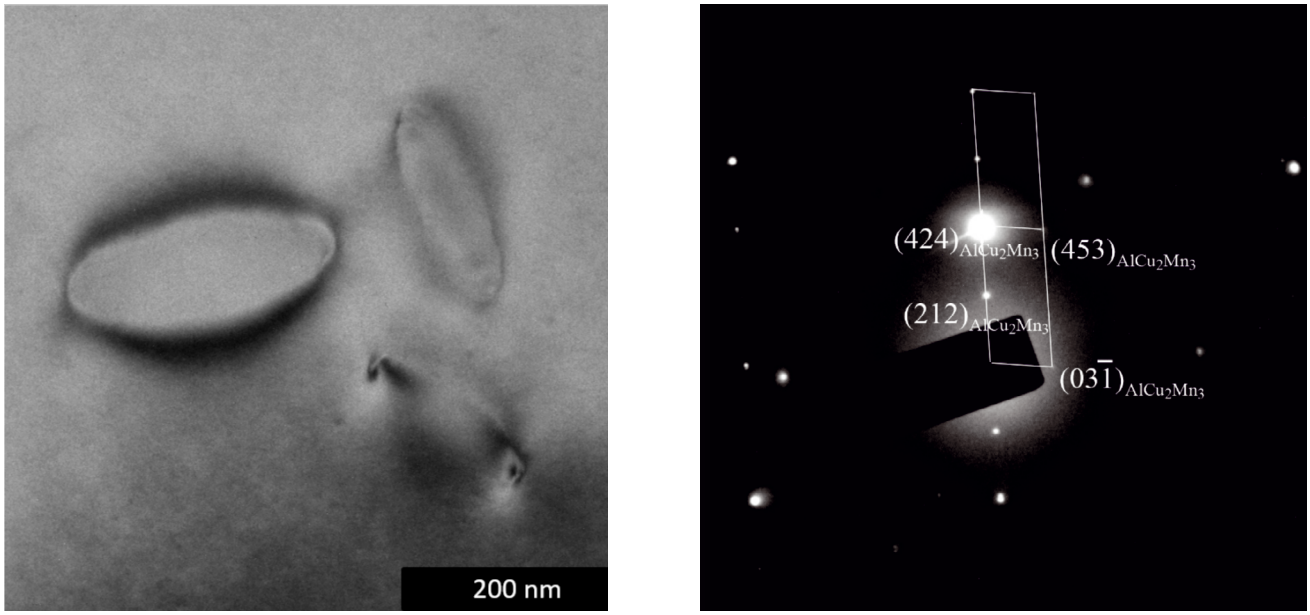

a *b*

Fig. 7. $Al_{20}Cu_2Mn_3$ particle:
particle image (*TEM*) (*a*), electron diffraction pattern (zone axis [7–2–6]) (*b*)

It should be noted that in the *ALTEK* alloys, phases other than the $Al_{20}Cu_2Mn_3$ type are present in insignificant amounts. The diffraction peak intensities of the Al_2CuMg and Al_6Mn phases are comparable to the background, indicating their low concentration. However, the combined application of *EDS* analysis and *Thermo-Calc* computations confirmed the presence of these phases in all studied alloys; therefore, they are marked on the diffraction patterns (Figs. 4, 5).

$Al_3(Sc,Zr,Hf)$ particles were not detected by *XRD* analysis, which is explained by the extremely low *Sc* content, making their detection and identification particularly difficult.

Conclusion

1. The effect of complex transition metal (*TM*) additions was investigated for the following alloys: *2% Cu-2% Mn-1.5% Mg* (**Base**), ***Base0.15Zr0.05Sc0.05Hf***, ***Base0.1Zr0.14Sc0.16Hf***, ***Base0.1Zr0.2Sc0.16Hf***, and ***Base0.1Zr0.25Sc0.16Hf***. It was established that significant grain refinement does not occur at *Sc* contents of 0.05–0.14 %. In alloys containing 0.20 and 0.25 % *Sc*, an equiaxed grain structure was formed with average grain diameters of 41.8 μm and 29.7 μm, respectively.

2. *Al_6Mn* and *Al_2CuMg* phase inclusions were identified by scanning electron microscopy (*SEM*) in all studied alloys. Furthermore, this method enabled the detection of primary *$Al_3(Sc,Zr,Hf)$* particles in alloys containing 0.20–0.25 % *Sc*, which were not resolvable by X-ray diffraction (*XRD*) analysis due to their low concentration and volume fraction.

References

1. Sizyakov V., Bazhin V., Vlasov A. Status and prospects for growth of the aluminum industry. *Metallurgist*, 2010, vol. 54, pp. 409–414. DOI: 10.1007/s11015-010-9316-z.

2. Belov N.A., Naumova E.A., Akopyan T.K. *Evtekticheskie splavy na osnove alyuminiya: novye sistemy legirovaniya* [Eutectic alloys based on aluminum: new alloying systems]. Moscow, Ruda i metally Publ., 2016. 256 p. ISBN 978-5-98191-083-8.

3. Dar S.M., Liao H. Creep behavior of heat resistant Al–Cu–Mn alloys strengthened by fine (θ′) and coarse ($Al_{20}Cu_2Mn_3$) second phase particles. *Materials Science and Engineering: A*, 2019, vol. 763, p. 138062. DOI: 10.1016/j.msea.2019.138062.

4. Feng Z.Q., Yang Y.Q., Huang B., Li M., Chen Y.X., Ru J.G. Crystal substructures of the rotation-twinned T ($Al_{20}Cu_2Mn_3$) phase in 2024 aluminum alloy. *Journal of Alloys and Compounds*, 2014, vol. 583, pp. 445–451. DOI: 10.1016/j.jallcom.2013.08.200.

5. Li X., Chen X., Feng Y., Chen B. Characterization and theoretical calculations of the T (Al20Cu2Mn3)/Al interface in 2024 alloys: TEM and DFT studies. *Vacuum*, 2023, vol. 210, pp. 111884. DOI: 10.1016/j.vacuum.2023.111884.

6. Belov N.A. [Substantiation of the composition and structure of deformable alloys based on the Al–Cu–Mn (Zr) system that do not require homogenization and hardening]. *Innovatsionnye tekhnologii, oborudovanie i material'nye zagotovki v mashinostroenii* [Innovative technologies, equipment and materials for blanking productions in mechanical engineering]. International Conference. Collection of works. Moscow, 2022, pp. 10–13. (In Russian).

7. Petrova A.N., Rasposienko D.Yu., Astafyev V.V., Yakovleva A.O. Structure and strength of Al-Mn-Cu-Zr-Cr-Fe ALTEC alloy after radial-shear rolling. *Letters on Materials*, 2023, vol. 13 (2), pp. 177–182. DOI: 10.22226/2410-3535-2023-2-177-182.

8. Fridlyander I.N., Berstenev V.V., Tkachenko E.A., Goloviznina G.M., Latushkina L.V., Lantsova L.P. Effect of heat treatment and deformation on the grain size and mechanical properties of duralumin-type alloys. *Metal Science and Heat Treatmen*t, 2003, vol. 45, pp. 239–245. DOI: 10.1023/A:1027316015223.

9. Belov N.A., Korotkova N.O., Akopyan T.K., Pesin A.M. Phase composition and mechanical properties of Al–1.5%Cu–1.5%Mn–0.35%Zr(Fe, Si) wire alloy. *Journal of Alloys and Compounds*, 2019, vol. 782, pp. 735–746. DOI: 10.1016/j.jallcom.2018.12.240.

10. Napalkov V.I., Frolov V.F., Baranov V.N., Belyaev S.V., Bezrukikh A.I. *Plavlenie i lit'e alyuminievykh splavov* [Melting and casting of aluminum alloys]. Krasnoyarsk, Siberian Federal University Publ., 2020. 716 p. ISBN 978-5-7638-4269-2.

11. Elagin V.I. *Legirovanie deformiruemykh alyuminievykh splavov perekhodnymi metallami* [Alloying of wrought aluminum alloys with transition metals]. Moscow, Metallurgiya Publ., 1975. 248 p.

12. Nokhrin A.V., Gryaznov M.Yu., Shotin S.V., Nagicheva G., Chegurov M.K., Bobrov A.A., Kopylov V.I., Chuvildeev V.N. Effect of Sc, Hf, and Yb additions on superplasticity of a fine-grained Al-0.4%Zr alloy. *Metals*, 2023, vol. 13, p. 133. DOI: 10.3390/met13010133.

13. Davydov V.G., Elagin V.I., Zakharov V.V., Rostova D. Alloying aluminum alloys with scandium and zirconium additives. *Metal Science and Heat Treatment*, 1996, vol. 38, pp. 347–352. DOI: 10.1007/bf01395323.

14. Drits A.M., Aryshenskii E.V., Kudryavtsev E.A., Zorin I.A., Konovalov S.V. Issledovanie raspada peresyshchennogo tverdogo rastvora v vysokomagnievykh alyuminievykh splavakh so skandiem, legirovannykh gafniem [The study of supersaturated solid solution decomposition in magnesium-rich aluminum alloys with scandium and hafnium additions]. *Frontier Materials & Technologies*, 2011, no. 4, pp. 38–48. DOI: 10.18323/2782-4039-2022-4-38-48.

15. Zorin I.A., Aryshenskii E.V., Kudryavtsev E.A., Drits A.M., Konovalov S.V. Vliyanie gafniya na vysokomagnievye splavy, legirovannye perekhodnymi metallami, pri termicheskoi obrabotke [The influence of hafnium on high-magnesium alloys doped with transition metals during heat treatment]. *Frontier Materials & Technologies*, 2024, no. 1, pp. 29–36. DOI: 10.18323/2782-4039-2024-1-67-3.

16. Zakharov V.V., Filatov Yu.A. Ekonomnolegirovannye skandiem alyuminievye splavy [Aluminum alloys sparingly alloyed with scandium]. *Tekhnologiya legkikh splavov = Technology of Light Alloys*, 2025, vol. 28, no. 4. DOI: 10.24412/0321-4664-2021-4-31-37.

17. Ragazin A.A., Aryshenskii E.V., Zorin I.A., Kudryavtsev E.A., Drits A.M., Konovalov S.V. Effect of hafnium on the microstructure formation during high-temperature treatment of high-magnesium aluminum alloys microalloyed with scandium and zirconium. *Physical Mesomechanics*, 2025, vol. 28, pp. 535–546. DOI: 10.1134/S1029959924601702.

18. Toleuova A.R., Belov N.A., Chervyakova V.V., Alabin A.N. Quantitative analysis of the Al–Cu–Mn–Zr phase diagram as a base for deformable refractory aluminum alloys. *Metal Science and Heat Treatment*, 2012, vol. 54 (7), pp. 402–406. DOI: 10.1007/s11041-012-9521-4.

19. Belov N.A., Alabin A.N. Energy efficient technology for Al–Cu–Mn–Zr sheet alloys. *Materials Science Forum*, 2013, vol. 765, pp. 13–17. DOI: 10.4028/www.scientific.net/MSF.765.13.

20. Belov N., Alabin A., Aleshchenko A., Mann V., Tsydenov K. Simultaneous increase of electrical conductivity and hardness of Al–1.5 wt.% Mn alloy by addition of 1.5 wt.% Cu and 0.5 wt.% Zr. *Metals*, 2019, vol. 9 (12), p. 1246. DOI: 10.3390/met9121246.

21. Belov N.A., Alabin A.N., Matveeva I.A. Optimization of phase composition of Al–Cu–Mn–Zr–Sc alloys for rolled products without requirement for solution treatment and quenching. *Journal of Alloys and Compounds*, 2014, vol. 583, pp. 206–213. DOI: 10.1016/j.jallcom.2013.08.202.

22. Malygin G.A. Prochnost' i plastichnost' nanokristallicheskikh materialov i nanorazmernykh kristallov [Strength and plasticity of nanocrystalline materials and nanosized crystals]. *Uspekhi fizicheskikh nauk = Physics-Uspekhi*, 2011, vol. 181, no. 11, pp. 1129–1156. DOI: 10.3367/UFNr.0181.201111a.1129. (In Russian).

23. Petrova A.N., Klenov A.I., Brodova I.G., Rasposienko D.Yu., Pil'shchikov A.A., Orlova N.Yu. Vliyanie tekhnologicheskikh faktorov na strukturu i svoistva Al–Cu–Mg–Si-splava, poluchennogo selektivnym lazernym splavleniem [Influence of technological factors on the structure and properties of Al–Cu–Mg–Si alloy obtained by selective laser melting]. *Fizika metallov i metallovedenie = Physics of Metals and Metallography*, 2023, vol. 124, no. 10, pp. 961–970. DOI: 10.31857/S0015323023600922.

24. Mondal C., Mukhopadhyay A.K. On the nature of T($Al_2Mg_3Zn_3$) and S(Al_2CuMg) phases present in as-cast and annealed 7055 aluminum alloy. *Materials Science and Engineering: A*, 2005, vol. 391 (1–2), pp. 367–376. DOI: 10.1016/j.msea.2004.09.013.

25. Chen Z., Li Z., Zhao K., Zhang H., Nagaumi H. Dendrite morphology evolution of Al_6Mn phase in suction casting Al–Mn alloys. *Materials*, 2020, vol. 13 (10), p. 2388. DOI: 10.3390/ma13102388.

26. Kang H., Li X., Su Ya., Liu D., Guo J., Fu H. 3-D morphology and growth mechanism of primary Al_6Mn intermetallic compound in directionally solidified Al-3at.%Mn alloy. *Intermetallics*, 2020, vol. 23, pp. 32–38. DOI: 10.1016/j.intermet.2011.12.015.

27. Lombardi A., Mu W., Ravindran C., Dogan N., Barati M. Influence of Al_2Cu morphology on the incipient melting characteristics in B206 Al alloy. *Journal of Alloys and Compounds*, 2018, vol. 747, pp. 131–139. DOI: 10.1016/j.jallcom.2018.02.329.

Conflicts of Interest

The authors declare no conflict of interest.